



Analysis and spatial prediction of water retention curves in two types of soil¹

Análise e previsão espacial de curvas de retenção de água em dois tipos de solo

Diego L. Cortés-Delgadillo^{2,3}, Jesús H. Camacho Tamayo^{3*} & Ramón Giraldo⁴

¹ Research developed at Universidad Nacional de Colombia, Bogotá, Colômbia

² Corporación Colombiana de Investigación Agropecuaria/Centro de Investigación Obonuco, Bogotá, Colômbia

³ Universidad Nacional de Colômbia/Facultad de Ingeniería/Departamento de Ingeniería Civil y Agrícola, Bogotá, Colômbia

⁴ Universidad Nacional de Colômbia/Facultad de Ciencias/Departamento de Estadística, Bogotá, Colômbia

HIGHLIGHTS:

Elevated compaction and the micropores flattened retention curves.

Slight field capacity - permanent wilting point difference.

Ground-based data (GF) demonstrate excellent accuracy for Andisols and for Oxisols at different depths.

ABSTRACT: Soil is a medium that stores and transfers air, water, nutrients and heat to microorganisms and plants. Its water storage capacity is studied by analysing water retention curves (WRCs), which establish the relationship between soil water content and the force with which water is retained. The objective of this work was to evaluate the capacity of functional geostatistics in predicting the spatial distribution of water retention curves in two types of soils. Experimental areas with two types of soil, Andisol and Oxisol, were selected, and a regular grid of 75 sites was established, from which water retention curves were obtained at two depths. The curves were subjected to geostatistical functional analysis (GF), and the applicability of this method was evaluated by obtaining the usable water table (LAA) and comparing the results with experimental data obtained using traditional methods. Based on cross-validation, it was verified that GF produced a better fit for the Andisol since the coefficient of determination between the LAA values for the measured data and predictions was high, with an R^2 of 99%; however, the proposed methodology was also reliable for the Oxisol, since an R^2 of 94% was obtained at the two depths studied.

Key words: usable water, spatial variability, functional data, functional kriging

RESUMO: O solo é um sistema que armazena e transfere ar, água, nutrientes e calor para microrganismos e plantas. Sua capacidade de armazenamento de água é estudada analisando a curva de retenção de água (WRC), que estabelece a relação entre a umidade do solo e a força com que ela é retida. O objetivo deste trabalho foi avaliar a capacidade preditiva da geoestatística funcional na distribuição espacial das curvas de retenção de água em dois tipos de solos. Foram selecionadas duas áreas experimentais, um Andisol e um Oxisol, nas quais foi estabelecida uma grade regular com 75 pontos, das quais foram obtidas curvas de retenção de água em duas profundidades. As curvas foram submetidas à análise geoestatística funcional (GF), sua aplicabilidade foi avaliada obtendo a tabela de água utilizável (LAA) e sua posterior análise espacial por métodos tradicionais nos quais os resultados foram comparados com os dados experimentais. Com base na validação cruzada, verificou-se que o uso de GF tem um melhor ajuste para o Andossolo, uma vez que o coeficiente de determinação entre os valores de LAA obtidos com os dados observados e aqueles obtidos com as previsões foi alto, com R^2 de 99%; no entanto, para o Latossolo, a metodologia proposta também é confiável, uma vez que foi obtido um R^2 de 94% nas duas profundidades estudadas.

Palavras-chave: variabilidade espacial, água útil, dados funcionais, kriging funcional



INTRODUCTION

Agricultural soils behave as complex systems that store and transport air, water, nutrients, and heat to microorganisms and plants (Kaur et al., 2021). Porosity plays an important role in a soil's water storage capacity because the presence of small water-filled pores require plants to exert greater force to extract the water (Howe & Peyton-Smith, 2021).

Studies of soil water retention curves (WRCs) establish links between stored water and the force that is needed to retain it. Commonly studied critical soil water contents include field capacity (FC), which is measured after the soil has lost water due to gravity, and the permanent wilting point (PWP), which occurs after plants have already taken in available water and cannot absorb more water from the soil.

Recently, several studies have been conducted that employed alternative methods for performing spatial analysis through which spatial predictions can be made at each measurement site that has a known curve but no specific data points (Sajedi-Hosseini et al., 2018; Chen et al., 2019; Padarian et al., 2022). These methods, known as functional geostatistics (GF) (Mateu & Giraldo, 2022), require the application of smoothing techniques to convert the discrete data from each site into continuous functions. Using GF analysis, it is possible to perform spatial interpolation on these curves.

In this study, GF was applied to WRCs to obtain usable water contents to evaluate the predicative capacity of GF and its potential use as a tool for describing the spatial variability in WRCs. Next, a cross-validation analysis was performed (using sites where data were already measured) to estimate prediction errors and compare them with the traditional univariate prediction methods that are often used for spatial analysis. Thus, the objective of this work was to evaluate the predictive capacity of functional geostatistics and its potential as a tool for describing the spatial variability in water retention curves in two types of soils.

MATERIALS AND METHODS

Two experimental locations were selected for this study. The first is in the municipality of Mosquera (Cundinamarca) at geographical coordinates of 4° 42' N and 74° 12' W, with an altitude of 2,543 m.a.s.l. The average mean temperature at this site is 13.1 °C, and the average annual precipitation is 670 mm. The site is part of the Bogotá River basin, which contains soil from the Marengo series, and the soil is classified as a Typic Melanudand with silty-loam and clay-loam textures and slopes of less than 1%. The soil is an Andisol with a thick, dark Ap horizon that originates from lake sediments with a small amount of volcanic ash and is supported by alluvial clay characterized by naturally poor and incomplete drainage, salinity problems, and low sodium contents. The experimental unit was 3.1 ha⁻¹ and was used for crops and grazing activities (Figure 1A).

The second sampling zone was located in the municipality of Puerto López, Meta, Colombia (4° 22' 38.50" N and 72° 13' 24.53" W, with an altitude of 156 m.a.s.l.). Precipitation

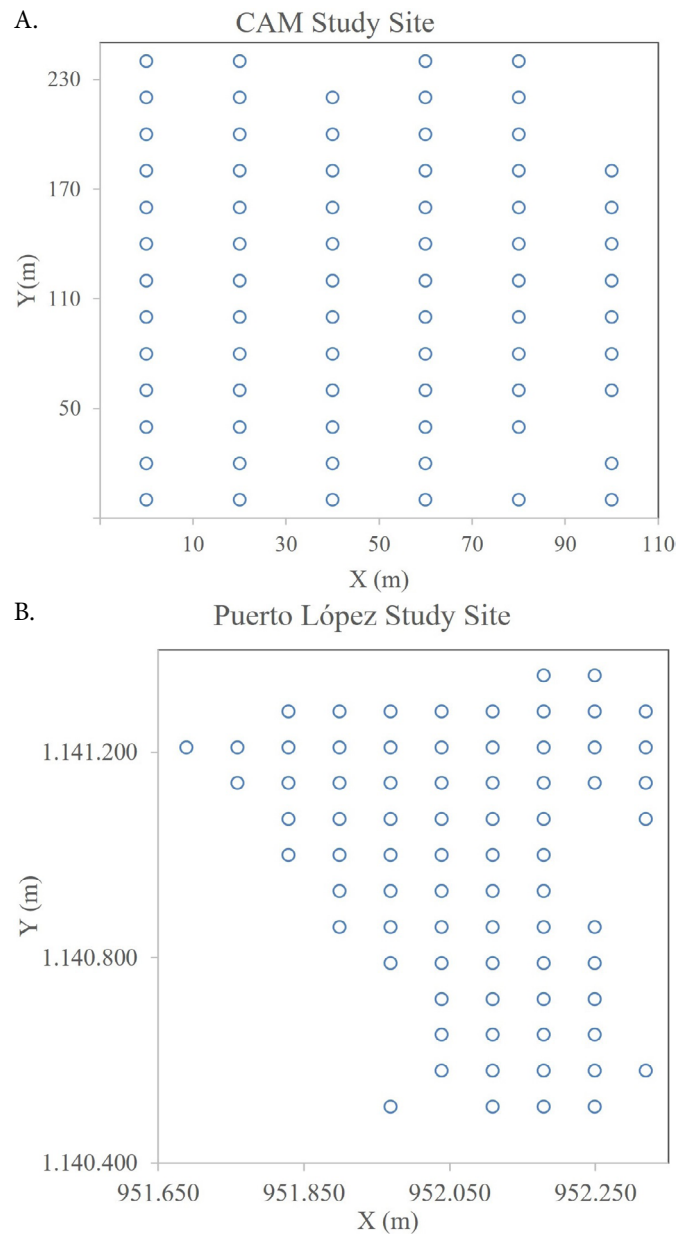


Figure 1. Experimental sites: Marengo Agricultural Center, Mosquera, Cundinamarca (A) and Puerto López, Meta (B)

in this zone follows a monomodal regime with an annual average of 2,375 mm; the mean temperature is 27 °C, and the relative humidity is 75% (Jaimes et al., 2003). The most predominant soil in this zone is a Typic Haplustox, which contains a thick layer of topsoil with a fine, loamy, silty texture and a slightly inclined slope (<5%). This soil is susceptible to physical degradation due to extensive ranching activities on the native meadows. The experimental unit covered 37 ha and was used for growing corn during the sampling period (Figure 1B).

In both zones, sampling was performed at two depths (0 to 10 cm and 10 to 20 cm) by using an evenly spaced grid with 75 measurement locations. To determine the soil water retention curves at each sampling site, membrane equipment and pressure cookers were used at pressures of 0.1, 0.3, 0.5, 1, 3, 5, 10, and 15 bar, as well as at the saturation point (0 bar). In addition, soil water content was determined at each pressure. The mean curve was determined for each depth and the two

soil types, and the differences between the values of the WRC at each measurement site and the averages of these values were calculated to obtain an “error curve” for each site. In addition, soil water retention was evaluated at the study sites by using the mean WRCs obtained at each depth.

B-splines (Zheng & Chen, 2022) were used in this study to estimate the error curves at each of the 75 measurement sites. Next, these curves were subjected to functional kriging (Mateu & Giraldo, 2022) by removing one error curve at a time and performing functional kriging on the remaining 74 curves to predict the “missing” curve, which resulted in the “observed” curve (estimated using B-splines) and the predicted curve for the unmeasured site (using functional kriging). The WRC was calculated at each site by fitting the calculated average curve with a correction from the “error” curve that was predicted at each site. A group of 75 measured WRCs and 75 predicted WRCs was generated, which allowed (leave-one-out) for cross-validation analysis to be performed. This procedure is useful for evaluating the quality of a method (the smaller the difference between the estimations and predictions, the better the method) and for comparing this method with traditional alternatives.

The functional kriging predictor is defined as follows (Giraldo et al., 2010):

$$\hat{\chi}(s_0) = \sum_{i=1}^n \lambda_i \chi(s_i); \lambda_1, \dots, \lambda_n \in \mathbb{R} \quad (1)$$

where $\chi(s_0)$ is the predicted curve at site s_0 , $\chi(s_i)$ corresponds to the curve observed at site s_i , and $i = 1, 2, \dots, n$ and $\lambda_i, i = 1, \dots, n$, are the weighting parameters that indicate the contributions of each observed curve to the predicted curve.

The λ_i parameters are estimated by solving the following system of equations (Giraldo et al., 2010):

$$\begin{pmatrix} \int_T \gamma_t(\|s_1 - s_1\|) dt & \dots & \int_T \gamma_t(\|s_1 - s_n\|) dt & 1 \\ \vdots & \ddots & \vdots & \vdots \\ \int_T \gamma_t(\|s_n - s_1\|) dt & \dots & \int_T \gamma_t(\|s_n - s_n\|) dt & 1 \\ 1 & \dots & 1 & 0 \end{pmatrix} \begin{pmatrix} \lambda_1 \\ \vdots \\ \lambda_n \\ -\mu \end{pmatrix} = \begin{pmatrix} \int_T \gamma_t(\|s_0 - s_1\|) dt \\ \vdots \\ \int_T \gamma_t(\|s_0 - s_n\|) dt \\ 1 \end{pmatrix} \quad (2)$$

where the integrals correspond to the trace-variogram function (Giraldo et al., 2010) evaluated for the distances between the observation sites (matrix to the left of the equal sign) and the distances between the observation sites and the prediction site (vector to the right of the equal sign). These integrals are calculated by estimating the trace-variogram function that is given by the following expression (Giraldo et al., 2010):

$$\hat{\gamma}(h) = \frac{1}{2|N(h)|} \sum_{i,j \in N(h)} \int_T (\chi_t(s_i) - \chi_t(s_j))^2 dt \quad (3)$$

where $N(h) = \{(s_i, s_j): \|s_i - s_j\| = h\}$ corresponds to the number of pairs of sites separated by hours and its subsequent fit with traditional parametric semivariance models (spherical, exponential, Gaussian, Matérn).

Using the measured curves and those obtained using functional prediction, available water content (AWC) was calculated at each site and for each soil. AWC was defined as the difference between the water contents at the FC and PWP at pressures of 0.3 and 15 bar, respectively (Melián et al., 2023).

The results obtained from functional kriging were compared with those obtained using univariate kriging at two depths. To perform a conventional analysis, the semivariance function was calculated for values of AWC and according to Cressie (1993), as follows:

$$\hat{\gamma}(h) = \frac{1}{2|N(h)|} \sum_{i=1}^{n(h)} [z(x_i) - z(x_i + h)]^2 \quad (4)$$

where $z(x_i)$ is the value of the LAA at point x_i , $z(x_i + h)$ is the value of LAA at a point with a distance of h from the previous point, and $N(h)$ is the number of pairs of data separated by the distance h . Next, this semivariogram is fit using one of the theoretical semivariance models mentioned earlier. Various criteria are considered for selecting the best model, including the coefficient of determination (R^2), the least sum of squared errors (LSSE) and the cross-validation correlation (CVC). The shared parameters among the theoretical semivariance models include the nugget (C_0), which is a discontinuity in the semivariogram at the origin, the variance of the process (C), and the reach (r), which is the distance to a spatial correlation. In addition, the nugget-variance ratio, $C/(C_0+C)$, is often used as a criterion for model selection. This parameter establishes the degree of spatial dependence (DSD) expressed by the attribute under study. Cambardella et al. (1994) state that the dependence is strong if the DSD is greater than 75%, is moderate for values between 25 and 75%, and is weak for values less than 25%. For all estimations and data processing, R version 4 was used with the libraries Geofd, fda and geor.

RESULTS AND DISCUSSION

Figure 2 shows that in both cases, the soil demonstrated flat WRCs with similar behaviours at each studied depth and small differences between the FC and PWP, which indicated the presence of a large number of micropores and that soil compaction occurred (Villalobos-Baquero & Meza-Montoya, 2019).

The curves obtained in both types of soil are common among loamy soils according to the findings of Tarazona-Meza et al. (2022), who observed FC and PWP values of $0.23 \text{ cm}^3 \text{ cm}^{-3}$ and $0.19 \text{ cm}^3 \text{ cm}^{-3}$ in an Oxisol and $0.30 \text{ cm}^3 \text{ cm}^{-3}$ and $0.26 \text{ cm}^3 \text{ cm}^{-3}$ in an Andisol at both depth ranges. In addition, these values were similar to those reported by Vargas-Díaz et al. (2022), Zhang et al. (2020) and Gómez-Rodríguez et al. (2013).

The increased prevalence of clays in the Andisol signifies an increased presence of micropores, as documented in this

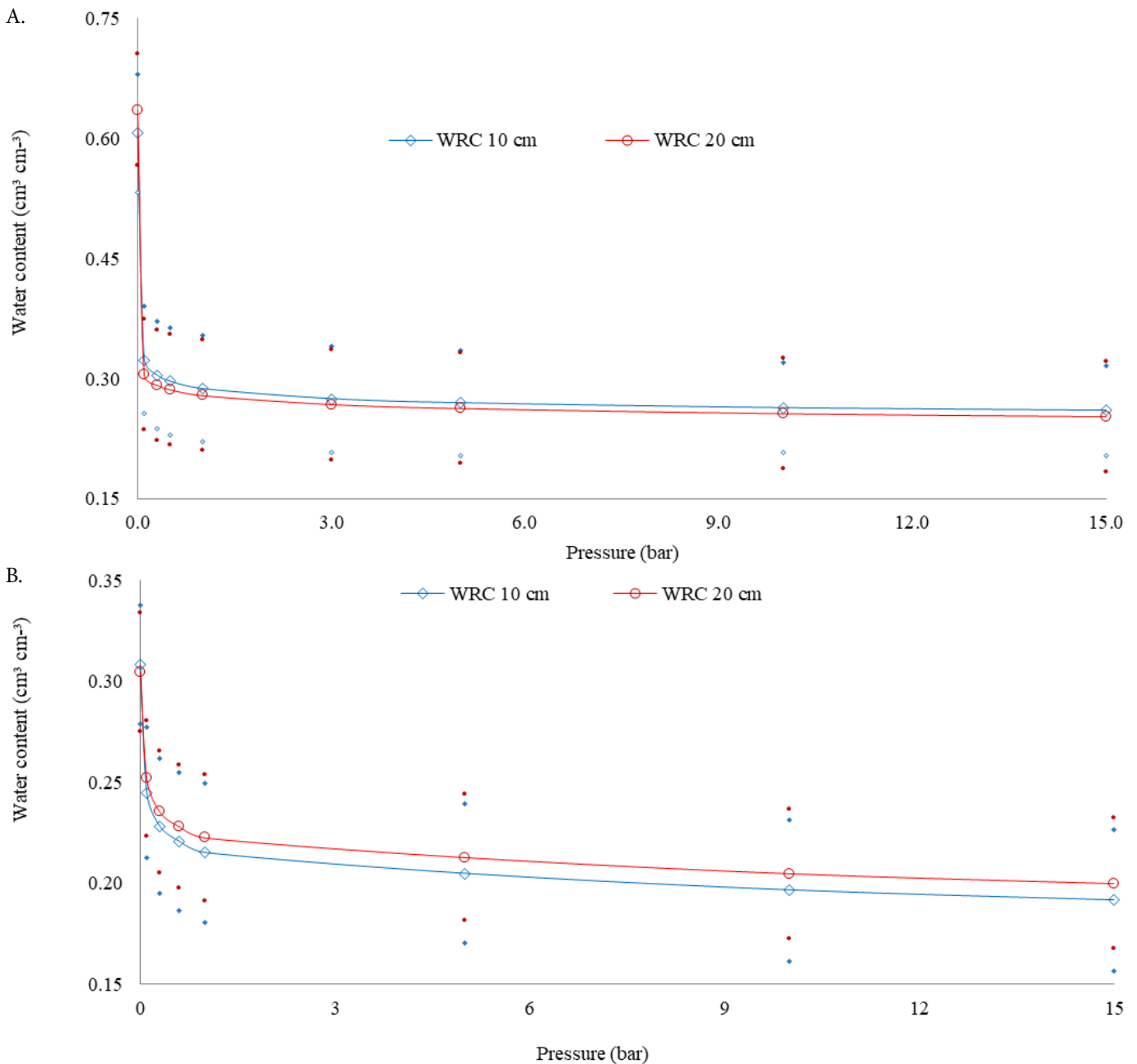


Figure 2. Average water retention curves of the Andisol (A) and Oxisol (B)

region by Varón-Ramírez et al. (2018). Consequently, a close arrangement of solid particles and a reduced prevalence of macropores are evident in the Andisol compared to the Oxisol. This results in more pronounced capillarity in the Andisol, leading to enhanced interactions with water. This, in turn, results in a predominance of water retention over water drainage at lower tensions, as observed in the research conducted by Silva et al. (2022). This phenomenon leads to greater water storage capacity, as depicted in the obtained curves.

The WRCs obtained for both soils do not follow general trends, which demonstrates a lack of homogeneity in the data (Figure 3). Thus, within the study zones, the water retention behaviours at some sites are noticeably different from the rest. Nevertheless, the curves show the same asymptotic patterns in the desaturation zones with respect to FC.

To understand the behaviour of the study zones more clearly, descriptive measures for FC and PWP were calculated

(Table 1). In both soils, the WRCs behaved similarly at both depths with respect to these measures. As seen in Figure 3, for the Andisol, the FC varied between approximately 0.13 cm³ cm⁻³ and 0.55 cm³ cm⁻³, and in the Oxisol, the FC varied between approximately 0.06 cm³ cm⁻³ and 0.40 cm³ cm⁻³. The difference between the FC and PWP was greater in the Andisol, indicating greater water availability in the soil in the study area.

Overall, the water contents at FC and the PWP showed mean variability at both depths, with CVs between 12 and 60%. This finding corresponded with the findings of Warrick & Nielsen (1980) and could be attributed to the degree of disturbance that the soil has undergone.

WRC predictions were performed at the 75 measurement sites. The measured and predicted curves for the Andisols are shown in Figure 3, and those for the Oxisols are shown in Figure 4. In both cases, few differences were found between the two sets of curves.

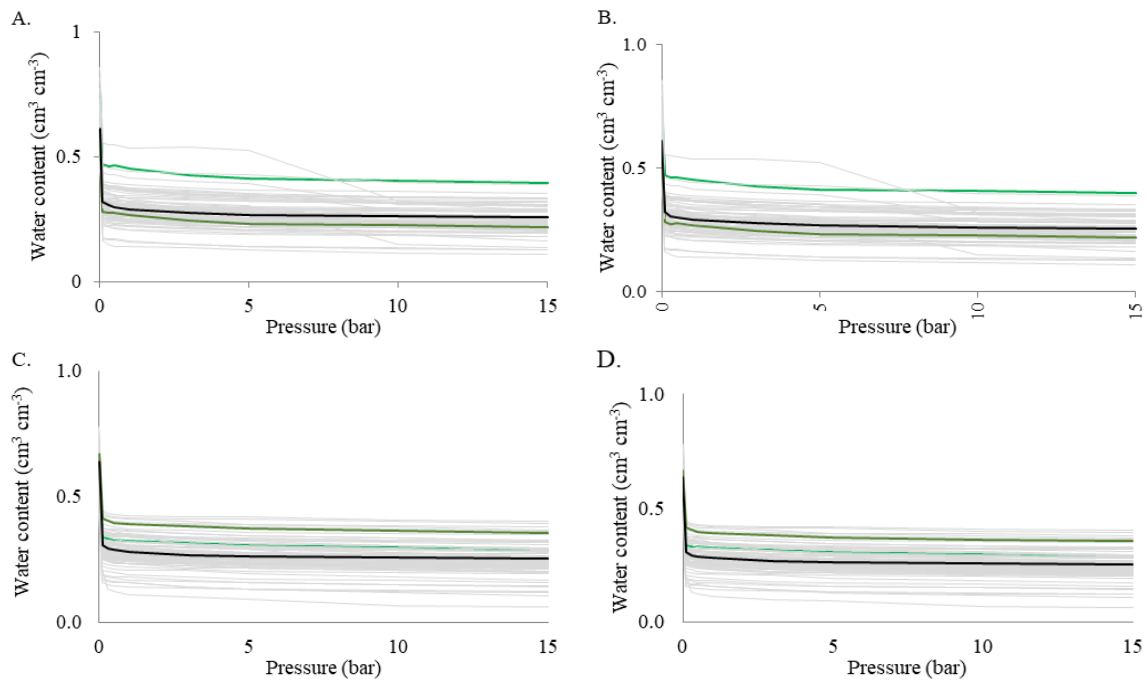


Figure 3. Measured water retention curves. A. at 10 cm and C. 20 cm. Water retention curves predicted using functional kriging B. at 10 cm and D. 20 cm in the Andisol

Table 1. Descriptive measurements of CC and PMP at depths of 0 to 10 cm and 10 to 20 cm in Andisols and Oxisols

	Depth (cm)	Mean	Median	CV (%)	Min	Max
CC	10And	0.31	0.30	21.9	0.15	0.55
	20And	0.29	0.29	22.1	0.13	0.43
	100x	0.23	0.24	14.7	0.12	0.29
	200x	0.24	0.23	12.8	0.15	0.29
PMP	10And	0.25	0.25	22.6	0.11	0.40
	20And	0.25	0.24	26.5	0.06	0.40
	100x	0.19	0.20	18.3	0.09	0.25
	200x	0.20	0.20	16.1	0.11	0.26

Using measured data and predicted curves at each site, the available water content (AWC) was calculated as the difference between the water contents at FC and the PWP. This value served as a numerical indicator of the goodness-of-fit when a simple linear regression was performed to compare the measured and predicted values at each site. In addition, this value indicated which soil type was most suited for GF analysis to predict WRCs. The resulting regressions are shown in Figure 5. A strong correlation was observed between the observations and predictions. The coefficient of determination was higher

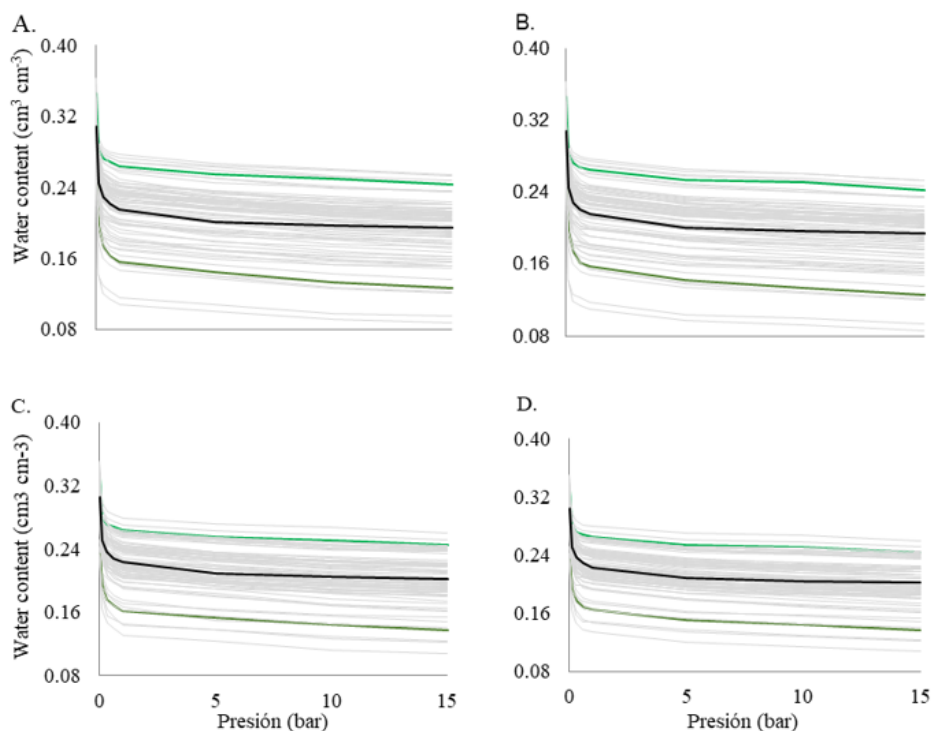


Figure 4. Measured water retention curves A. at 10 cm and C. 20 cm. Water retention curves predicted using functional kriging B. at 10 cm and D. 20 cm in the Oxisol

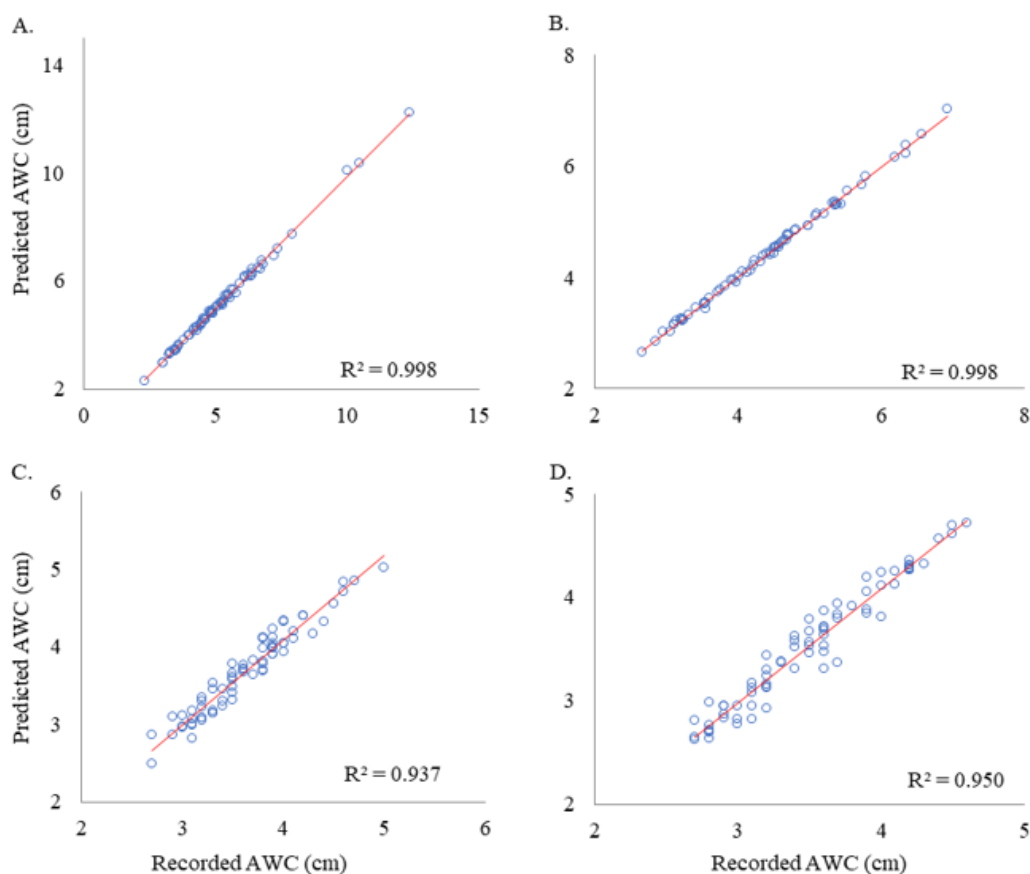


Figure 5. Cross-validation of available water content (AWC). Andisol 10 (A) and 20 cm (B); Oxisol 10 (C) and 20 cm (D)

in the Andisol (0.99) than in the Oxisol (0.94) at both depths. Despite the high R^2 value of the Oxisol, greater data scatter was observed. The values of R^2 indicated that more than 99% (Andisol) and 94% (Oxisol) of the measured data could be explained by the proposed predictor.

The model might have performed better for the Andisol because this soil has a higher content of organic matter and a higher clay content compared to the Oxisol. Organic matter content as well as clay content affects the pedotransfer functions and, as presented in this study, alters the water retention curves since organic matter and clays affect the presence and distribution of pores in the soil (Albuquerque et al., 2022; Veloso et al., 2023).

The zones analysed in this study show high levels of compaction and an elevated presence of micropores, which were inferred from the trends and flattened shape of the soil water retention curves, with a small difference between FC and the PWP.

To evaluate the applicability of functional geostatistics in predicting data from water retention curves, geostatistical parameters were determined (Table 2), and spatial distribution maps were generated (Figures 6 and 7) for the values of AWC that were calculated using the measured data and the data obtained from the predictor.

For both soils and at both soil depths, the generated geostatistical parameters were similar, which demonstrated the goodness of fit of the functional predictor used in this study. The experimental and functional kriging-predicted AWC data fit the theoretical semivariogram models well, with the Andisol fitting the spherical models and the Oxisol fitting the exponential models at both depths.

At 0-10 cm in the Andisol, the AWC showed a moderate DSD, and the values of C_0 were relatively far from zero. At 10-20 cm in the Andisol and at both depths in the Oxisol, the C_0 values were much closer to zero, which indicated a strong spatial dependence that was also evidenced by DSD values

Table 2. Theoretical semivariogram parameters fit to the observed and predicted available water content for horizons at 0 to 10 cm and 10 to 20 cm

Soil	Model	C_0	$C_0 + C$	Range (m)	CVC	DSD	
Andisol	AWC _{Obs10}	Spherical	1.386	2.975	98.0	0.99	0.53
	AWC _{Pre10}	Spherical	1.307	2.862	96.9	0.99	0.54
	AWC _{Obs20}	Spherical	0.007	0.951	30.3	0.65	0.99
	AWC _{Obs20}	Spherical	0.006	0.934	31.9	0.63	0.99
Oxisol	AWC _{Obs10}	Exponential	0.000	0.204	163.8	0.92	1.00
	AWC _{Pre10}	Exponential	0.000	0.250	169.2	0.85	0.99
	AWC _{Obs20}	Exponential	0.000	0.243	313.5	0.99	1.00
	AWC _{Obs20}	Exponential	0.026	0.352	560.4	1.03	0.93

CVC - Cross-validation correlation; DSD - Degree of spatial dependence

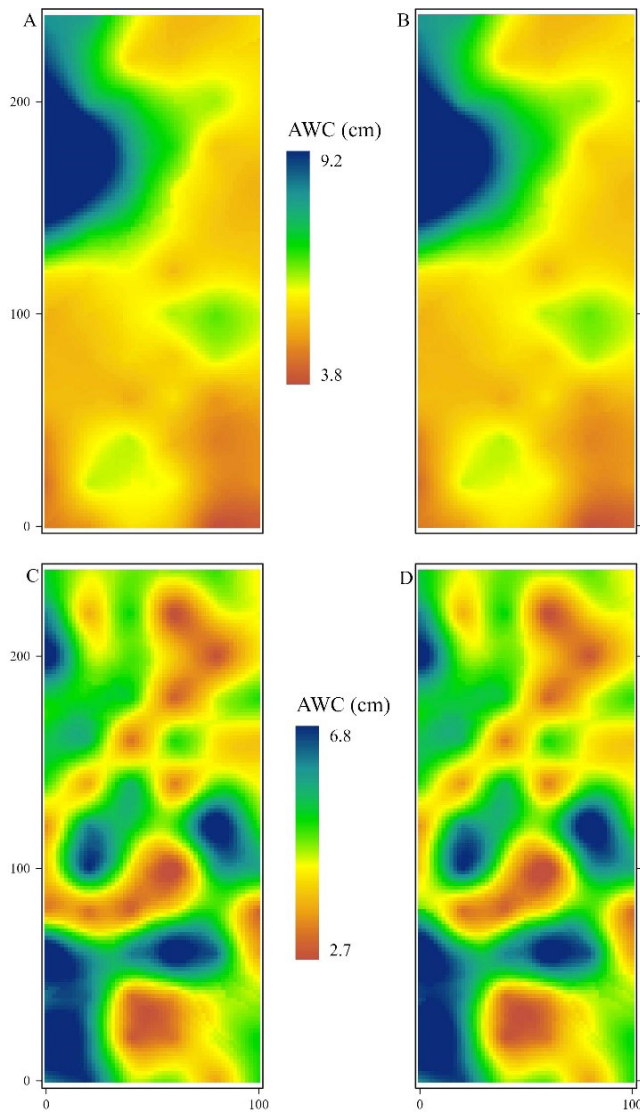


Figure 6. Distribution maps for the available water content (AWC) in Andisol. Observed AWC at 10 cm (A), predicted AWC at 10 cm (B), observed AWC at 20 cm (C) and predicted AWC at 20 cm (D)

above 75% (Birol & Günal, 2022). These results indicate that the sampling distances were adequate, since when greater distances between points exist, the variograms tend to present larger nugget due to the intrinsic properties of the soil, which also results in greater estimation errors when spatial pedotransfer functions are developed (Castrignano et al., 2023), causing the sill to exceed the sampling variance, especially in areas that present different soil types as well as different levels of anthropogenic intervention (Camacho-Tamayo et al., 2008; Heydari et al., 2023).

The maps show the high spatial variability found in the soil relative to the properties analysed (Figures 6 and 7). The maps created from the values generated using functional kriging are consistent with the measured data maps, which show a spatial distribution that is similar to that of the measured data based on the minimal differences between the two sets of maps. The Oxisol shows somewhat more notable differences between the maps, with a CVC of 0.94, which is lower than that obtained for the Andisol.

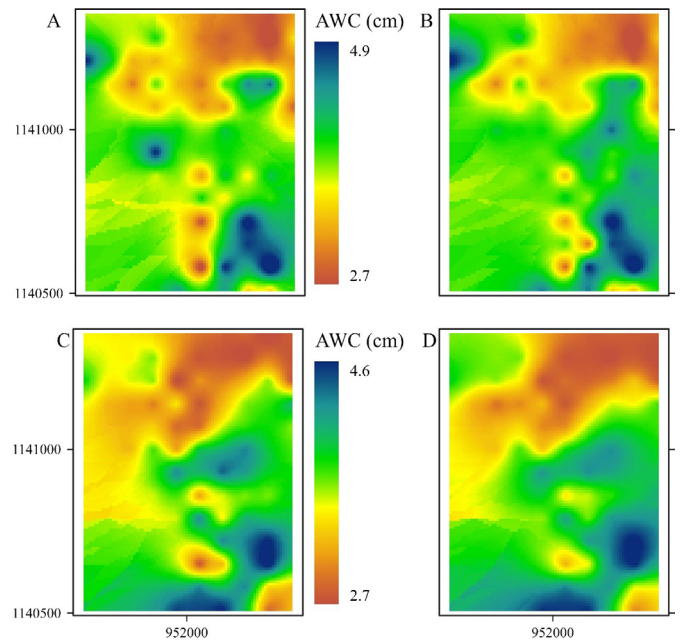


Figure 7. Distribution maps for the available water content in the Oxisol. Observed AWC at 10 cm (A), predicted AWC at 10 cm (B), observed AWC at 20 cm (C) and predicted AWC at 20 cm (D)

CONCLUSIONS

1. The results of the cross-validation analysis show that the use of functional geostatistics results in better fits for the Andisol at both depths given the high coefficient of determination between the available water content (AWC) values obtained from the measured data and the predicted data ($R^2 = 99\%$). The proposed methodology is reliable for Oxisols as well ($R^2 = 94\%$) at the two studied depths.

2. The maps created from the predicted water retention curves also exhibited behaviour similar to that of the maps obtained from the field-measured data. Similarly, map fitting was better in the areas where the Andisol is located in comparison to the areas with the Oxisol.

LITERATURA CITED

- Albuquerque, E.A.C.; de Faria Borges, L.P.; Brasil Cavalcante, A.L.; Lemos Machado, S. Prediction of soil water retention curve based on physical characterization parameters using machine learning. *Soil and Rocks*, v.45, e2022000222, 2022. <http://doi.org/10.28927/SR.2022.000222>
- Birol, M.; Günal, H. Field scale variability in soil properties and silage corn yield. *Soil Studies*, v.11, p.27-34, 2022. <http://doi.org/10.21657/soilst.1143238>
- Camacho-Tamayo, J.H.; Luengas, C.A.; Leiva, F.R. Effect of agricultural intervention on the spatial variability of some soils chemical properties in the eastern plains of Colombia. *Chilean journal of agricultural research*. v.68, p.42-55, 2008.
- Cambardella, C. A.; Moorman, T.B.; Novak, J. M.; Parkin, T.B.; Karlen, D. L.; Turco, R. F.; Konopka, A. E. Field-scale variability of soil properties in Central Iowa Soils. *Soil Science Society of America Journal*, v.58, p.1501-1511, 1994. <https://doi.org/10.2136/sssaj1994.03615995005800050033x>

- Castrignanò, A.; Heydari, L.; & Bayat, H. Scale-dependent field partition based on water retention functional data. *Land*, v.12, p.1106, 2023. <https://doi.org/10.3390/land12051106>
- Chen, W.; Panahi, M.; Khosravi, K.; Pourghasemi, H. R.; Rezaie, F.; & Parvinnezhad, D. Spatial prediction of groundwater potentiality using ANFIS ensembled with teaching-learning-based and biogeography-based optimization. *Journal of Hydrology*, v.572, p.435-448, 2019. <https://doi.org/10.1016/j.jhydrol.2019.03.013>
- Cressie, N. *Statistics for spatial data*. 1ed.; John Wiley & Sons, Inc., Wiley Series in Probability and Statistics, 1993. <https://doi.org/10.1002/9781119115151>
- Giraldo, R.; Delicado, P.; Mateu, J. Continuous time-varying Kriging for spatial prediction of functional data: an environmental application, *Journal of Agricultural, Biological, and Environmental Statistics* v.15, p.66-82, 2010. <https://doi.org/10.1007/s13253-009-0012-z>
- Gómez-Rodríguez, K.; Camacho-Tamayo, J. H.; Vélez-Sánchez, J. E.; Changes in water availability in the soil due to tractor traffic. *Engenharia Agrícola*, v.33, p.1156-1164, 2013.
- Heydari, L., Bayat, H. & Castrignanò, A. Scale-dependent geostatistical modelling of crop-soil relationships in view of Precision Agriculture. *Precision Agriculture*, v.24, p.1261-1287, 2023. <https://doi.org/10.1007/s11119-023-09989-5>
- Howe, J. A.; Peyton-Smith, A. The soil habitat. In: Gentry, T. J.; Fuhrmann, J. J.; Zuberer D. A. *Principles and Applications of Soil Microbiology*, Elsevier, 2021, Cap.2, p.23-55.
- Jaimes, W.; Navas, G.; Salamanca, C.; Conde, A. Estudio detallado de suelos de la estación experimental de Corpoica "Sabanas" en la Altillanura Colombiana. *Corpoica, C. I. La Libertad, Villavicencio, Colombia*, v.62, p.1-9, 2003.
- Kaur, T.; Devi, R.; Kour, D.; Kour, D.; Yadav, A.; Yadav, A.N., Dikilitas, M.; Abdel-Azeem, A.; Ahluwalia, A.; Saxena, A. Plant growth promoting soil microbiomes and their potential implications for agricultural and environmental sustainability. *Biologia*, v.76, p.2687-2709, 2021. <https://doi.org/10.1007/s11756-021-00806-w>
- Mateu, J.; Giraldo, R. Introduction to Geostatistical Functional Data Analysis. In: Mateu, J.; Giraldo, R. *Geostatistical Functional Data Analysis*. Wiley Series in Probability and Statistics. 2022. Cap.1, p.1-25.
- Melián, E.; Gatica, G.; Pucheta, E. Compromisos de rasgos del leño en plantas del desierto: un modelo triangular para comprender las variaciones intra e interespecíficas a lo largo de un gradiente de aridez. *Austral Ecology*, v.1, p.1-16, 2023. <https://doi.org/10.1111/aec.13370>
- Padarian, J.; Stockmann, U.; Minasny, B.; McBratney, A. Monitoring changes in global soil organic carbon stocks from space. *Remote Sensing of Environment*, v.281, p.113260, 2022. <https://doi.org/10.1016/j.rse.2022.113260>
- Sajedi-Hosseini, F.; Choubin, B.; Solaimani, K., Cerdà, A.; Kavian, A. Spatial prediction of soil erosion susceptibility using a fuzzy analytical network process: Application of the fuzzy decision making trial and evaluation laboratory approach. *Land degradation & development*, v.29, p.3092-3103, 2018. <https://doi.org/10.1002/ldr.3058>
- Silva, F. G.; De Assis Junior, R. N.; Shiso Toma, R.; De Sousa Oliveira, L.; Da Silva Marques, E.; Anunciato Mota, J. C. Physical-hydraulic attributes as indicators of functionality of soil pores under different compaction levels. *Revista Caatinga*, v.35, p.884-893, 2022. <https://doi.org/10.1590/1983-21252022v35n416rc>
- Tarazona-Meza, N.; Chavarría-Párraga, J.; Moreira-Saltos, J. El cultivo de maíz y sus necesidades hídricas en Manabí, Ecuador. *Revista de Ciencias Agropecuarias ALLPA*, v.5, p.2-11, 2022. <https://publicacionescd.uleam.edu.ec/index.php/allpa/article/view/349>
- Vargas Diaz, R. E.; Wilches Ortiz, W. A.; Espitia Malagón, E. M. Efecto del establecimiento de sistemas de rotación para el cultivo de la papa sobre las características químicas y físicas del suelo. *Siembra*, v.9, p.1-9, 2022. <https://doi.org/10.29166/siembra.v9i2.4023>
- Varón-Ramírez, V.M.; Camacho-Tamayo, J.H.; González-Nivia, J. Management zones determination based on physical properties of the soil. *Ciência & Agrotecnologia*, v.42, p.248-260, 2018. <http://dx.doi.org/10.1590/1413-70542018423002318>
- Veloso, M. F.; Rodrigues, L. N.; Fernandes Filho, E. I.; Veloso, C. F.; Rezende, B. N. Pedotransfer functions for estimating the van Genuchten model parameters in the Cerrado biome. *Revista Brasileira de Engenharia Agrícola e Ambiental*, v.27, p.202-208, 2023. <https://doi.org/10.1590/1807-1929/agriambi.v27n3p202-208>
- Villalobos-Barquero, V.; Meza-Montoya, A. Impacto en la densidad aparente del suelo provocado por el tránsito de búfalos (*Bubalus bubalis*) en arrastre de madera. *Revista de Ciencias Ambientales*, v.53, p.147-155, 2019. <https://dx.doi.org/10.15359/rca.53-2.8>
- Warrick, A. W.; Nielsen, D. R. Spatial variability of soil physical proprieties in field, HILLEL, D. *Applications of soil physics*, Academic Press, 1980.
- Zhang, X.; Wendroth, O.; Matocha, C.; Zhu, J.; Reyes, J. Assessing field-scale variability of soil hydraulic conductivity at and near saturation. *Catena*, v.187, p.1-11, 2020. <https://doi.org/10.1016/j.catena.2019.104335>
- Zheng, Y.; Chen, F. Volumetric parameterization with truncated hierarchical B-splines for isogeometric analysis. *Computer Methods in Applied Mechanics and Engineering*, v.401, p.1-19, 2022. <https://doi.org/10.1016/j.cma.2022.115662>